

Impact of relativistic effects on the primordial non-Gaussianity signature in the large-scale clustering of quasars

Mike (Shengbo) Wang¹,^{*} Florian Beutler^{2,1} and David Bacon¹

¹*Institute of Cosmology and Gravitation, University of Portsmouth, Burnaby Road, Portsmouth PO1 3FX, UK*

²*Institute for Astronomy, University of Edinburgh, Royal Observatory, Blackford Hill, Edinburgh EH9 3HJ, UK*

In original form 2020 July 3

ABSTRACT

Relativistic effects in clustering observations have been shown to introduce scale-dependent corrections to the galaxy over-density field on large scales, which may hamper the detection of primordial non-Gaussianity f_{NL} through the scale-dependent halo bias. The amplitude of relativistic corrections depends not only on the cosmological background expansion, but also on the redshift evolution and sensitivity to the luminosity threshold of the tracer population being examined, as parametrized by the evolution bias b_e and magnification bias s . In this work, we propagate luminosity function measurements from the extended Baryon Oscillation Spectroscopic Survey (eBOSS) to b_e and s for the quasar (QSO) sample, and thereby derive constraints on relativistic corrections to its power spectrum multipoles. Although one could mitigate the impact on the f_{NL} signature by adjusting the redshift range or the luminosity threshold of the tracer sample being considered, we suggest that, for future surveys probing large cosmic volumes, relativistic corrections should be forward modelled from the tracer luminosity function including its uncertainties. This will be important to quasar clustering measurements on scales $k \sim 10^{-3} h^{-1} \text{Mpc}$ in upcoming surveys such as the Dark Energy Spectroscopic Instrument (DESI), where relativistic corrections can overwhelm the expected f_{NL} signature at low redshifts $z \lesssim 1$ and become comparable to $f_{\text{NL}} \simeq 1$ in the power spectrum quadrupole at redshifts $z \gtrsim 2.5$.

Key words: cosmology: observations – cosmological parameters – large-scale structure of Universe

1 INTRODUCTION

It is known that primordial non-Gaussianity (PNG), which encodes dynamics of the inflationary period in the early Universe, leaves an imprint in the large-scale structure (LSS) at late times not only in higher-order statistics such as the bispectrum, but also in the clustering of virialized haloes by introducing a scale-dependent modification to the large-scale tracer bias (Dalal et al. 2008; Matarrese & Verde 2008; Slosar et al. 2008). For the local type of PNG f_{NL} , although the strongest constraint yet comes from observations of the cosmic microwave background (CMB) by *Planck*¹ ($f_{\text{NL}} = 0.9 \pm 5.1$; Planck Collaboration, Akrami et al. 2019), upcoming LSS probes such as the Dark Energy Spectroscopic Instrument² (DESI) and *Euclid*³ are forecast to offer competitive constraints with uncertainties of $O(1)$ (Font-Ribera et al. 2014; Amendola et al. 2018; Mueller et al. 2018), with current galaxy surveys such as the ex-

tended Baryon Oscillation Spectroscopic Survey⁴ (eBOSS) already achieving uncertainties of $O(10)$ (Castorina et al. 2019).

Despite the relativistic nature of gravitational theories governing structure formation, the Newtonian description of fluctuations in the distribution of galaxies is usually adequate as relativistic effects are suppressed below the Hubble horizon scale. In the past, the modelling of fully relativistic galaxy clustering has been unnecessary to obtain cosmological parameter constraints, as cosmic variance dominates over any corrections. With the next generation of galaxy surveys probing far wider and deeper cosmic volumes, however, such approximate prescriptions might no longer be sufficient to attain unbiased constraints. The necessary relativistic corrections for galaxy clustering observations have been derived by Yoo et al. (2009), Bonvin & Durrer (2011) and Challinor & Lewis (2011). Many subsequent works have demonstrated their importance for constraining cosmological parameters, in particular f_{NL} , as its scale-dependent signature on large-scales can be disguised as relativistic effects (Bruni et al. 2012; Jeong et al. 2012; Bertacca et al. 2012; Camera et al. 2015; Alonso et al. 2015; Fonseca et al. 2015; Rac-

* Email: mike.wang@port.ac.uk

¹ esa.int/planck

² desi.lbl.gov

³ euclid-ec.org

⁴ sdss.org/surveys/eboss

canelli et al. 2016, 2018; Lorenz et al. 2018). On the other hand, the investigation of relativistic corrections in itself is a valuable exercise, as it offers tests of relativistic gravitational theories on cosmological scales, including the equivalence principle (Bonvin et al. 2020). Future galaxy surveys like DESI are forecast to deliver the first detections of these relativistic corrections (Beutler & Dio 2020).

One crucial aspect of relativistic corrections is that their total amplitude does not only depend on the cosmological and gravitational models, but also on the background number density of the tracer population being examined through its redshift evolution and sensitivity to the luminosity threshold of observations, as respectively captured by parameters known as the *evolution bias* b_e and *magnification bias* s . Previous works have mostly only considered relativistic effects in Fisher forecasts for f_{NL} by assuming fiducial values of b_e and s , but the exact dependence of these parameters on redshift and the luminosity threshold, as well as how their uncertainties propagate to the observed power spectrum, remains much less clear. In this work, we concretize these considerations for quasars (QSO), which are an ideal tracer for detecting f_{NL} thanks to their high redshift range and bias, and proceed as follows:

(i) We first review in section 2 general relativistic corrections in galaxy clustering to linear order, including contributions from evolution bias b_e and magnification bias s which we shall formally introduce. This motivates the need for determining tracer luminosity functions;

(ii) Based on the previous work by Palanque-Delabrouille et al. (2016), we fit the quasar luminosity function with eBOSS QSO measurements in section 3, before deriving constraints on b_e , s and thus relativistic corrections in section 4;

(iii) In section 5, we compare scale-dependent modifications to the quasar power spectrum due to relativistic corrections and due to f_{NL} at different redshifts for two different magnitude thresholds, and discuss in section 6 the need to include luminosity function constraints in forward modelling of relativistic clustering statistics for future galaxy surveys.

2 RELATIVISTIC CLUSTERING OF GALAXIES

While the Newtonian description of the galaxy over-density field δ is appropriate for observations on sub-horizon scales, as the clustering scale k^{-1} approaches the horizon scale \mathcal{H}^{-1} , where $\mathcal{H}(z)$ is the conformal Hubble parameter at redshift z , the observed field

$$\delta(\mathbf{r}, z) = b_1 \delta_m(\mathbf{r}, z) - \frac{1}{\mathcal{H}} \partial_r v_{\parallel}(\mathbf{r}, z) - \left(\frac{\mathcal{H}'}{\mathcal{H}^2} + \frac{2-5s}{\mathcal{H}\chi} + 5s - b_e \right) v_{\parallel}(\mathbf{r}, z) + \dots \quad (1)$$

receives relativistic corrections of $\mathcal{O}(\mathcal{H}/k)$ or higher that are otherwise suppressed. Here $'$ denotes a conformal time derivative, $b_1(z)$ is the scale-independent tracer bias with respect to the matter over-density field δ_m , $v_{\parallel} \equiv \mathbf{v} \cdot \hat{\mathbf{r}}$ is the component of peculiar velocity \mathbf{v} along the line of sight $\hat{\mathbf{r}}$, and $\chi(z)$ is the comoving distance. The quantities b_e , s are the evolution and magnification biases, which do not a priori follow from a background cosmological model but are rather derived at a given redshift from

$$b_e(z) = - \frac{\partial \ln \bar{n}(z; < \bar{m})}{\partial \ln(1+z)}, \quad (2a)$$

$$s(z) = \frac{\partial}{\partial m} \Big|_{\bar{m}} \lg \bar{n}(z; < m) \quad (2b)$$

with $\lg \equiv \log_{10}$, where $\bar{n}(z; < m)$ is the underlying comoving number density of the tracer population below a given absolute magnitude m , and \bar{m} is the absolute magnitude threshold of the observed tracer sample (Challinor & Lewis 2011).

Although equation (1) neglects lensing and gravitational potential contributions, it goes beyond modelling of only redshift-space distortions coupled to $\partial_r v_{\parallel}$; crucially, it includes Doppler contributions from the peculiar velocity v_{\parallel} itself, which in principle should leave a scale-dependent signature in large-scale galaxy clustering. This is easily seen in Fourier space under the plane-parallel approximation that $\mu \equiv \hat{\mathbf{k}} \cdot \hat{\mathbf{r}}$ does not vary with \mathbf{r} in the observed over-density field; with the help of the linear continuity equation

$$\mathbf{v}(\mathbf{k}) = -i \frac{\mathcal{H}}{k} f \delta_m(\mathbf{k}) \hat{\mathbf{k}}, \quad (3)$$

where $f(z)$ is the linear growth rate, we can recast equation (1) as

$$\delta(\mathbf{k}, z) = \left(b_1 + i \frac{\mathcal{H}}{k} g f \mu + f \mu^2 \right) \delta_m(\mathbf{k}, z), \quad (4)$$

where we have parametrized the anisotropic relativistic corrections by the dimensionless quantity

$$g(z) \equiv \frac{\mathcal{H}'}{\mathcal{H}^2} + \frac{2-5s}{\mathcal{H}\chi} + 5s - b_e. \quad (5)$$

We employ the Friedman equations⁵ to rewrite

$$\frac{\mathcal{H}'}{\mathcal{H}^2} = 1 - \frac{3}{2} \Omega_m, \quad (6)$$

where $\Omega_m(z)$ is the matter density parameter, and then split $g(z)$ into three contributions,

$$g(z) = \left(1 - \frac{3}{2} \Omega_m + \frac{2}{\mathcal{H}\chi} \right) - b_e + 5s \left(1 - \frac{1}{\mathcal{H}\chi} \right). \quad (7)$$

Here the first term depends only on the cosmological density parameters through the accelerating background expansion, whereas the second and third terms depend on the tracer sample in question through its evolution and magnification biases.

Therefore to determine the relativistic corrections in equation (1) or (4), two ingredients are needed: 1) a background cosmological model; 2) the tracer *luminosity function* $\phi(m, z)$ from which the underlying comoving number density

$$\bar{n}(z; < \bar{m}) = \int_{-\infty}^{\bar{m}} dm \phi(m, z) \quad (8)$$

below the absolute magnitude threshold \bar{m} can be derived – this is our focus in the next section.

3 QUASAR LUMINOSITY FUNCTION

Determining the tracer luminosity function is not only important for modelling relativistic corrections, it could also be a significant source of uncertainty for constraining PNG. In this work, we examine quasars as a single tracer for detecting f_{NL} thanks to their high tracer bias and redshift range. We attempt to recover their evolution and magnification biases from their luminosity function, before propagating these measurements to relativistic corrections to the power spectrum multipoles.

To this end, we consider eBOSS QSO luminosity function measurements obtained by Palanque-Delabrouille et al. (2016, Table A.1

⁵ We neglect radiation and spatial curvature.

therein) for the redshift range $0.7 < z < 4$, which are corrected for observational systematics such as completeness and bandpass redshifting of spectra (i.e. K -correction). We describe the empirical quasar luminosity function with the *pure luminosity evolution* (PLE) model (Boyle et al. 2000; Richards et al. 2006; Palanque-Delabrouille et al. 2016),

$$\phi(m, z) = \frac{\phi_*}{10^{0.4(\alpha+1)[m-m_*(z)]} + 10^{0.4(\beta+1)[m-m_*(z)]}}, \quad (9a)$$

which is a double power law with bright- and faint-end indices α, β that may differ depending on the redshift z relative to the pivot redshift $z_p = 2.2$. Here ϕ_* is the overall normalization constant, and

$$m_*(z) = m_*(z_p) - \frac{5}{2} \left[k_1(z - z_p) + k_2(z - z_p)^2 \right] \quad (9b)$$

is the characteristic absolute magnitude, where k_1, k_2 are redshift evolution parameters that can also differ between low redshift $z < z_p$ and high redshift $z > z_p$. Therefore this is a parametric model with 10 parameters, $\theta = \{\phi_*, m_*(z_p), \alpha_l, \beta_l, k_{1l}, k_{2l}, \alpha_h, \beta_h, k_{1h}, k_{2h}\}$, where subscripts ‘l’ and ‘h’ denote low redshift and high redshift respectively.

3.1 Likelihood function

Without re-performing the iterative luminosity function fitting procedure on the raw quasar count data in Palanque-Delabrouille et al. (2016), we adopt the likelihood inference approach outlined in Pozzetti et al. (2016) for simplicity. For absolute magnitude and redshift bins (m_i, z_i) indexed by i , the quasar number count \hat{N}_i follows the logarithmic probability density function (PDF)

$$\ln \mathbb{P}(\hat{N}_i | N_i) = \hat{N}_i \ln N_i - N_i - \ln \Gamma(\hat{N}_i) \quad (10)$$

with variance $\text{Var}(\hat{N}_i) = N_i$, where the expected number count is given by

$$N_i = \langle \hat{N}_i \rangle = \int_{\text{bin-}i} dz \frac{dV(z)}{dz} \int_{\text{bin-}i} dm \phi_\theta(m, z). \quad (11)$$

Here $\phi_\theta(m, z)$ is the PLE luminosity function (9) with model parameters θ and

$$dV(z) = 4\pi r^2 \frac{dr}{dz} dz \quad (12)$$

is the differential comoving volume, where $r(z)$ is the radial comoving distance.

To obtain an approximate likelihood for the parametric luminosity function model, we first note that the binned luminosity function $\hat{\phi} \propto \hat{N}$ and thus the estimated uncertainty on $\ln \hat{\phi}$ is $\sigma = \hat{N}^{-1/2}$. Expanding the PDF (10) around its maximum, we obtain the quadratic form

$$\ln \mathcal{L}(\theta) - \ln \mathcal{L}_{\max} \simeq -\frac{1}{2} \sum_i \frac{x_i^2}{\sigma_i^2}, \quad (13)$$

where $\sigma_i^2 = 1/\hat{N}_i$ and

$$x_i^2(\theta) = 2 \left[1 - \frac{\phi_\theta(m_i, z_i)}{\hat{\phi}_i} + \ln \frac{\phi_\theta(m_i, z_i)}{\hat{\phi}_i} \right]. \quad (14)$$

Therefore the likelihood function we shall use to infer the best-fitting PLE luminosity function model is

$$\ln \mathcal{L}(\theta) = - \sum_i \frac{1}{\sigma_i^2} \left[1 - \frac{\phi_\theta(m_i, z_i)}{\hat{\phi}_i} + \ln \frac{\phi_\theta(m_i, z_i)}{\hat{\phi}_i} \right], \quad (15)$$

where we have neglected the additive normalization constant.

Table 1. Posterior median estimates of the PLE model parameters (see equation 9) for the eBOSS QSO luminosity function.

Parameter	Redshift range	
	0.68–2.2	2.2–4.0
$\lg \phi_*$	−26.20 ^{+0.21} _{−0.20}	
$m_*(z_p)$	−5.76 ^{+0.09} _{−0.08}	
α	−3.27 ^{+0.17} _{−0.19}	−2.57 ^{+0.08} _{−0.09}
β	−1.40 ^{+0.06} _{−0.06}	−1.21 ^{+0.10} _{−0.09}
k_1	−0.10 ^{+0.08} _{−0.09}	−0.37 ^{+0.09} _{−0.09}
k_2	−0.40 ^{+0.06} _{−0.06}	−0.01 ^{+0.06} _{−0.06}

3.2 Best-fitting models

By sampling the PLE model parameters from the likelihood function (15) with the Markov chain Monte Carlo (MCMC) sampler ZEUS⁶ (Karamanis & Beutler 2020), we have re-fitted the quasar luminosity function from the eBOSS QSO measurements. Because of the exchange symmetry between the power-law indices α, β in equation (9a), we have imposed the constraint $\alpha < \beta$ to avoid a multi-modal posterior distribution. The PLE parameters are estimated by the sample posterior medians, as reported in Table 1, with a reduced chi-square value of $\chi^2/\text{d.o.f.} = 105/77 \approx 1.36$ per degree of freedom (d.o.f.).

We note that there appears to be some discrepancy between our fitted parameters and the results in Palanque-Delabrouille et al. (2016), so we compare both best-fitting models with the eBOSS QSO measurements in Fig. 1. In all redshift bins the two fitted models are in reasonable agreement with measurements and are virtually indistinguishable across a wide magnitude range. Noticeable differences only appear either at the very faint end below the limiting absolute magnitude corresponding to the g -band apparent magnitude cut $g = 22.5$,⁷ which is not constrained by any measurements, or at the very bright end, where uncertainties are comparatively large. We attribute such discrepancies to the fact that Palanque-Delabrouille et al. (2016) were able to fit the raw quasar number counts corrected for systematics whereas we have only fitted the binned luminosity function reported in their final results. As we shall see in the next section, constraints on the relativistic corrections propagated from these best-fitting luminosity function models are statistically consistent and have no significant impact on our analysis.

4 CONSTRAINTS ON RELATIVISTIC CORRECTIONS

Having determined the quasar luminosity function, we now proceed to constrain relativistic corrections to quasar clustering statistics by propagating the sampled luminosity function parameters in the form of MCMC chains to evolution and magnification biases. To do so, we specify the Planck15 Λ CDM cosmology with $(h, \Omega_{\Lambda,0}, \Omega_{m,0}) = (0.6790, 0.6935, 0.3065)$ (Planck Collaboration, Ade et al. 2016),

⁶ github.com/minaskar/zeus

⁷ The g -band apparent magnitude is normalized to the absolute magnitude $\bar{m}(z) = g - \mu(z) - [K(z) - K(z = 2)]$, where $\mu(z)$ is the distance modulus, $K(z)$ is the K -correction and the normalization redshift $z = 2$ is close to the median redshift of the eBOSS QSO sample (Palanque-Delabrouille et al. 2016).

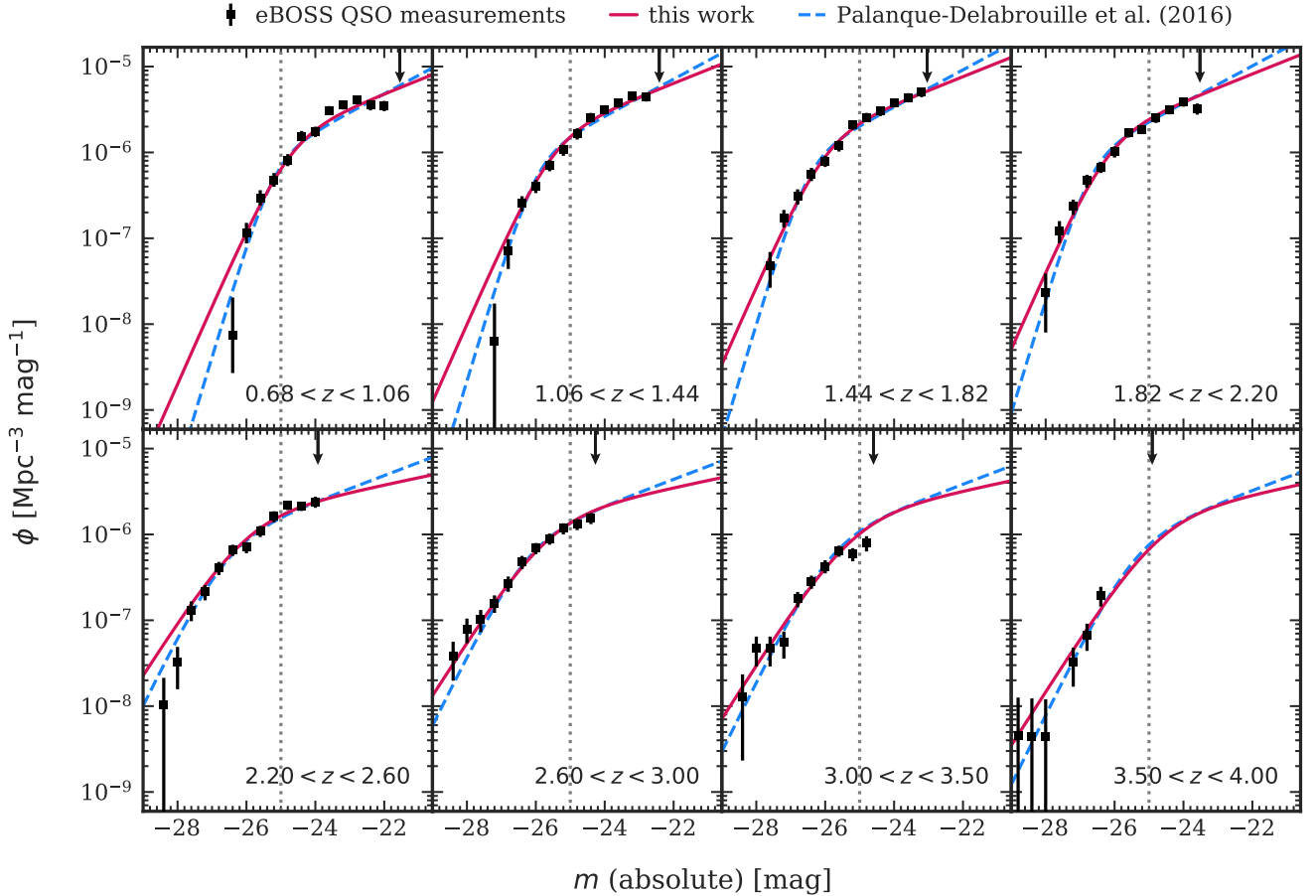


Figure 1. Best-fitting quasar luminosity functions under the PLE model (9) in eBOSS QSO redshift bins. Measurements with uncertainties and the best-fitting model shown in dashed blue lines are taken from Palanque-Delabrouille et al. (2016). The best-fitting model of this work (see Table 1) is shown in solid red lines. The downward pointing arrows mark the limiting absolute magnitude corresponding to the apparent magnitude cut $g = 22.5$ in each redshift bin. The vertical dotted lines mark the absolute magnitude threshold $\bar{m} = -25$ used in this work.

which is a choice consistent with Palanque-Delabrouille et al. (2016). We also specify a fiducial absolute magnitude threshold $\bar{m} = -25$ based on the last eBOSS QSO redshift bin.

4.1 Constraints on relativistic biases

We first compute the quasar comoving number density $\bar{n}(z)$ from equation (8) by numerically integrating our best-fitting luminosity function model $\phi(m, z)$ up to the absolute magnitude threshold \bar{m} . In Fig. 2, we show the derived measurements of $\bar{n}(z)$ from sampled luminosity function parameters within the 95% credible interval across the redshift range $0.7 < z < 4$; for the eBOSS QSO redshift bins, we also show the measurements of $\bar{n}(z)$ with error bars corresponding to the 68% credible interval. The small apparent discontinuity in $\bar{n}(z)$ corresponds to the pivot redshift z_p which is a feature of the empirical luminosity function model.

Next, we compute the evolution bias b_e and magnification bias s from equation (2) by numerical differentiation with redshift step size $\Delta z = 0.001$. We have found that, based on the eBOSS QSO luminosity function, b_e can be an order of magnitude larger than s , although both appear in relativistic corrections at the same order in equation (7). One interesting comparison one could make for $b_e(z)$ is with the analytic estimate from the universal mass function (UMF) of haloes, although the validity of this approach is only limited to

tracer sample selection that is insensitive to the halo merger history (Jeong et al. 2012). The evolution bias predicted from the UMF is given by

$$b_e(z) = \delta_c f(z) [b_1(z) - 1], \quad (16)$$

where $\delta_c \approx 1.686$ is the critical density of spherical collapse, and here we consider a simple redshift evolution model for the quasar linear bias $b_1(z) = 1.2/D(z)$, which is based on the DESI baseline survey (DESI Collaboration, Aghamousa et al. 2016) and does not account for possible luminosity dependence. Based on power-law fitting to observed quasar clustering amplitudes, studies have found that the luminosity dependence of quasar bias appears to be rather weak, at least at low and intermediate redshifts possibly because quasars reside in a broad range of haloes of different masses (White et al. 2012; Shen et al. 2013; Krolewski & Eisenstein 2015). However, some current models and observations hint at a greater level of luminosity dependence at higher redshifts and luminosity ranges, but such quasars are rare and the luminosity dependence of their bias can only be better constrained with larger future data sets (Shen 2009; Croton 2009; Conroy & White 2012; Timlin et al. 2018).

In Fig. 3, we show the derived measurements of b_e and s for $0.7 < z < 4$ within the 95% credible interval and their measurements in eBOSS QSO redshift bins with 68%-level uncertainties, together with the UMF prediction. As is the case with comoving number

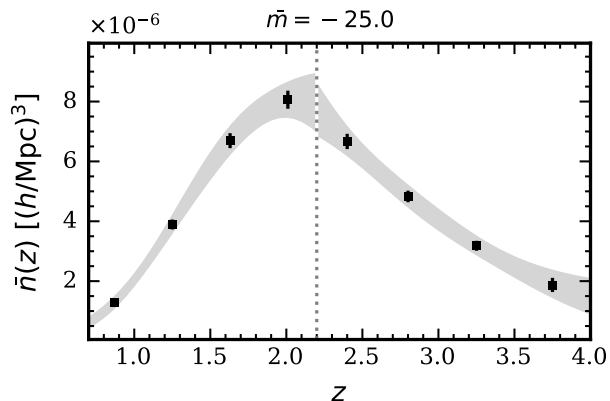


Figure 2. Derived measurements of the quasar comoving number density $\bar{n}(z)$ below the absolute magnitude threshold $\bar{m} = -25$ from the best-fitting eBOSS QSO luminosity function in this work (see Table 1). Data points with error bars are measurements within the 68% credible interval for the eBOSS QSO redshift bins. The shaded grey regions show the 95% credible interval. The vertical dotted line marks the pivot redshift $z_p = 2.2$.

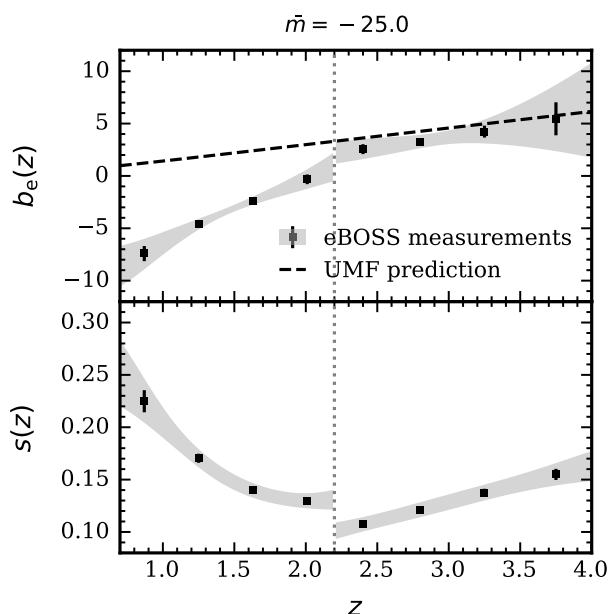


Figure 3. Derived measurements of evolution bias b_e and magnification bias s at the absolute magnitude threshold $\bar{m} = -25$ from the best-fitting eBOSS QSO luminosity function in this work (see Table 1). Data points with error bars are measurements within the 68% credible interval for the eBOSS QSO redshift bins. The shaded grey regions show the 95% credible interval. The vertical dotted lines mark the pivot redshift $z_p = 2.2$.

density, there is an apparent discontinuity in both parameters at the pivot redshift $z_p = 2.2$. We note that, although the UMF prediction is in reasonable agreement with our measurements at high redshifts, it does not capture the behaviour of the negative evolution bias values below redshift $z \approx 2$. This is perhaps unsurprising given the limitation of the UMF prediction and the simplicity of our quasar bias model.

In section 3.2, we have noted that our best-fitting luminosity function under the PLE model is somewhat discrepant from that of Palanque-Delabrouille et al. (2016), although the parameter estimates

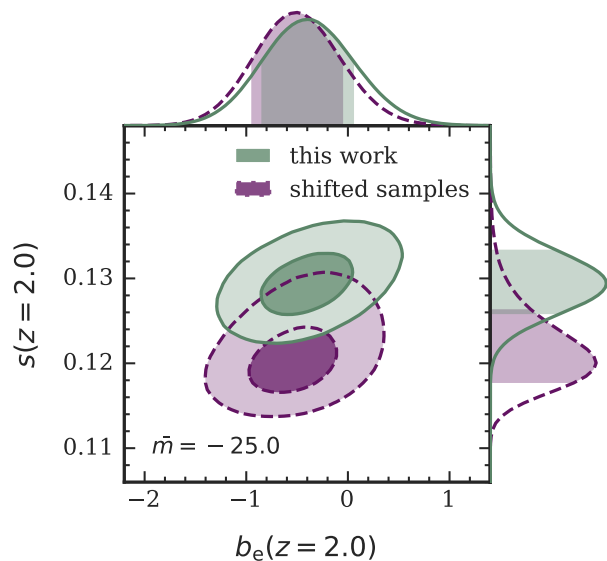


Figure 4. Constraints on evolution bias b_e and magnification bias s at redshift $z = 2$ and absolute magnitude threshold $\bar{m} = -25$ from the eBOSS QSO luminosity function under the PLE model (9). Solid green contours show the 68% and 95% credible regions of the joint posterior distribution sampled from the likelihood function (15) (this work). Dashed purple contours are from the same samples except shifted to coincide with the best-fitting PLE model parameters from Palanque-Delabrouille et al. (2016) (shifted samples). The shaded regions in the top and right panels show the 68% credible intervals of the marginal posterior distributions.

have similar uncertainties. To investigate the impact on the measured relativistic bias parameters, we shift our sampled luminosity function parameter chains so that the shifted posterior median estimates would coincide precisely with the best-fitting PLE parameters in Palanque-Delabrouille et al. (2016), and then we propagate the resultant parameter samples to constraints on b_e and s . In Fig. 4, we show that the joint (b_e, s) constraints at redshift $z = 2$ from our original parameter samples and the shifted samples are broadly consistent. This is particularly the case for evolution bias b_e , which we shall see dominates the relativistic corrections over magnification bias s . We have also checked that the joint (b_e, s) constraints from the original and shifted samples are consistent at other redshifts, e.g. $z = 0.87, 3.75$ which are respectively the lowest and highest eBOSS QSO redshift bins.

4.2 Constraints on the relativistic correction function

In section 2, we have shown that relativistic corrections to clustering statistics at different redshifts and scales are modulated by the function $g(z)$. Under the Planck15 cosmology, we can constrain $g(z)$ from relativistic bias measurements obtained above. In Fig. 5, we show the derived measurements of $\mathcal{H}g(z)$ within the 95% credible interval and its measurements in eBOSS QSO redshift bins with 68%-level uncertainties. Both the values and uncertainties of $g(z)$ are dominated by the contribution from evolution bias b_e , which can be an order of magnitude larger than $s(z)$ as shown in Fig. 3. This means that the slight discrepancy between our best-fitting luminosity function and that of Palanque-Delabrouille et al. (2016) is not of concern, as it mostly affects the magnification bias s rather than b_e . Coincidentally, $g(z)$ vanishes at around the pivot redshift $z_p = 2.2$,

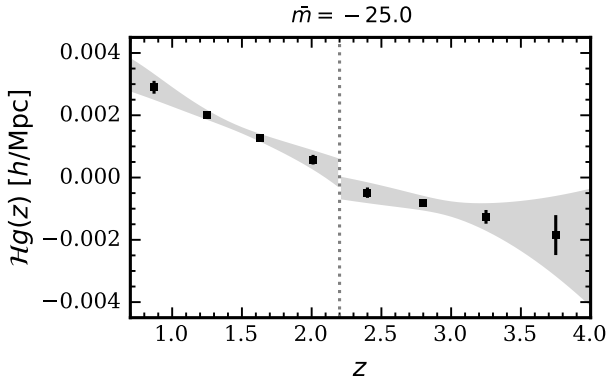


Figure 5. Derived measurements of the relativistic correction function $\mathcal{H}g(z)$ (see equation 7) at the absolute magnitude threshold $\bar{m} = -25$ from the best-fitting eBOSS QSO luminosity function in this work (see Table 1). Data points with error bars are measurements within the 68% credible interval for the eBOSS QSO redshift bins, and the shaded region shows the 95% credible interval. The vertical dotted line marks the pivot redshift $z_p = 2.2$.

so the small discontinuity from the empirical luminosity function model is also not of concern.

Having propagated quasar luminosity function measurements through to constraints on $g(z)$ that parametrizes relativistic corrections, we shall investigate in the following section how it modifies the quasar clustering power spectrum multipoles on large scales.

5 SCALE-DEPENDENT MODIFICATION TO POWER SPECTRUM MULTIPOLES

In the presence of local primordial non-Gaussianity f_{NL} , the linear tracer bias $b_1(z)$ receives a scale-dependent modification

$$\Delta b(k, z) = 3f_{\text{NL}}(b_1 - p) \frac{1.27\delta_c \Omega_{\text{m},0} H_0^2}{c^2 k^2 T(k) D(z)}, \quad (17)$$

where p is a parameter that depends on the tracer sample (here we adopt $p = 1.6$ for quasars), H_0 is the Hubble parameter at present, c is the speed of light, and $T(k)$ is the matter transfer function (Slosar et al. 2008). The numerical factor 1.27 arises as we normalize the linear growth factor $D(z)$ to unity at present. As $k \rightarrow 0$, $T(k) \rightarrow 1$ and $\Delta b \propto k^{-2}$, so the signature of f_{NL} is enhanced on large scales.

Under the plane-parallel approximation, Kaiser (1987) showed the anisotropic clustering power spectrum in redshift space is

$$P^{\text{K}}(k, \mu) = (b + f\mu^2)^2 P_{\text{m}}(k) \quad (18)$$

on large scales, where P_{m} is the linear matter power spectrum. By considering the Legendre multipoles with respect to the angle variable μ , $P^{\text{K}}(k, \mu)$ is equivalent to the combination of the monopole

$$P_0^{\text{K}}(k) = \left(b^2 + \frac{2}{3}bf + \frac{1}{5}f^2 \right) P_{\text{m}}(k), \quad (19a)$$

the quadrupole

$$P_2^{\text{K}}(k) = \left(\frac{4}{3}bf + \frac{4}{7}f^2 \right) P_{\text{m}}(k) \quad (19b)$$

and the hexadecapole $P_4^{\text{K}}(k)$ which we neglect as it does not depend on the tracer bias. Note that here the total bias b now includes both b_1 and the scale-dependent modification $\Delta b \propto k^{-2}$, which changes

the standard Kaiser multipoles P_{ℓ}^{K} with only the scale-independent bias b_1 by

$$\Delta P_0(k) = \left[\left(2b_1 + \frac{2}{3}f \right) \Delta b + \Delta b^2 \right] P_{\text{m}}(k), \quad (20a)$$

$$\Delta P_2(k) = \frac{4}{3} \Delta b f P_{\text{m}}(k). \quad (20b)$$

In contrast to the quadrupole which only receives a modification proportional to k^{-2} , the monopole receives modifications proportional to both k^{-2} and k^{-4} when $f_{\text{NL}} \neq 0$.

In section 2, we have shown that relativistic corrections similarly leave a scale-dependent signature. By considering the two-point function of expression (4), we see that relativistic corrections only change the Kaiser monopole and quadrupole by

$$\Delta P_0(k) = \frac{1}{3} \frac{\mathcal{H}^2}{k^2} g^2 f^2 P_{\text{m}}(k), \quad (21a)$$

$$\Delta P_2(k) = \frac{2}{3} \frac{\mathcal{H}^2}{k^2} g^2 f^2 P_{\text{m}}(k), \quad (21b)$$

which are proportional only to k^{-2} (Raccanelli et al. 2018). By comparing equations (20) and (21), one could foresee that relativistic corrections can mimic the effect of f_{NL} in both the monopole and quadrupole of the clustering power spectrum on large scales, except for the monopole on very large scales where $k \sim \mathcal{H}$ and the k^{-4} contribution would dominate over any k^{-2} contributions. The extent to which relativistic corrections can wash out the f_{NL} signature depends on the precise amplitude of $g(z)$.

Since we have obtained $g(z)$ constraints in the previous section, we can make a concrete comparison between the power spectrum multipole modifications due to f_{NL} and $g(z)$. To this end, we consider a fiducial value $f_{\text{NL}} = 1$ at which level different classes of inflation models can be distinguished (Maldacena 2003; Alvarez et al. 2014). As the fiducial case, we continue to adopt the Planck15 cosmology, the absolute magnitude threshold $\bar{m} = -25$ for the quasar sample and $b_1(z) = 1.2/D(z)$ as per the previous section.

In Fig. 6, we show the power spectrum multipoles for $k \in [10^{-4}, 10^{-1}] h^{-1} \text{Mpc}$ in the presence of these modifications at two redshifts $z = 0.87, 3.75$, which we recall are respectively the lowest and highest eBOSS QSO redshift bins. At the lower redshift, relativistic effects dominate over PNG effects and obscure the f_{NL} signature. At the higher redshift, although the relativistic modification is comparable to the f_{NL} effect in the quadrupole, the f_{NL} signature stands out in the monopole. This offers a hint that, at least for the quasar sample, pushing the upper redshift range may help mitigate any potential contamination of the f_{NL} signature from relativistic corrections.

Indeed, when we consider the relative amplitudes of relativistic and PNG modifications evolving with redshift, we find relativistic corrections have a less significant impact on the f_{NL} signature in the power spectrum monopole at high redshift. In Fig. 7, we compare the relativistic and PNG modifications ΔP_{ℓ} to the power spectrum multipoles as a fraction of the standard Kaiser prediction P_{ℓ}^{K} across the eBOSS QSO redshift range $0.7 < z < 4$ at a fixed wave number $k = 10^{-3} h^{-1} \text{Mpc}$ – this is close to the largest scale which DESI and *Euclid* may access (Aghamousa et al. 2016; Laureijs et al. 2011). In addition to our fiducial absolute magnitude threshold $\bar{m} = -25$, we also consider a less conservative cut at $\bar{m} = -22$, which is the limiting magnitude of the lowest eBOSS QSO redshift bin. For both cases, we find that relativistic corrections dominate over the effect of f_{NL} at lower redshifts $z \lesssim 1$, and values of $\Delta P_{\ell}/P_{\ell}^{\text{K}}$ due to relativistic effects and f_{NL} reach parity at some redshift between 1 and 2. Although relativistic modifications to the quadrupole become

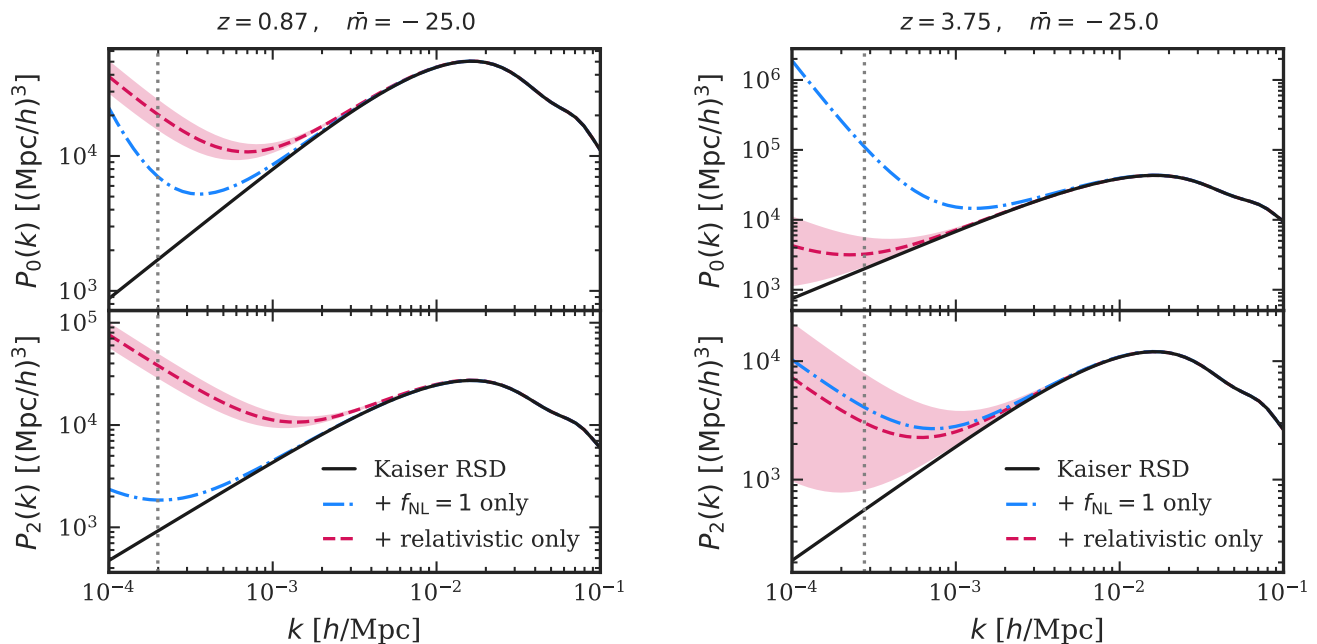


Figure 6. Large-scale quasar clustering power spectrum monopole $P_0(k)$ and quadrupole $P_2(k)$ at redshift $z = 0.87$ (left column) and $z = 3.75$ (right column) with magnitude threshold $\bar{m} = -25.0$. The Kaiser RSD model is shown by the solid black lines. The effect of relativistic corrections without local non-Gaussianity f_{NL} is shown by the dashed red lines with the shaded red regions showing the 95% credible interval derived from the best-fitting eBOSS QSO luminosity function in this work (see Table 1). The effect of $f_{\text{NL}} = 1$ (fiducial value) without relativistic corrections is shown by the dash-dotted blue lines. The vertical dotted lines mark the horizon scale $k = \mathcal{H}$.

comparable to the f_{NL} effect again at higher redshift $z \gtrsim 2.5$ given its widening uncertainties, the f_{NL} signature in the monopole remains mostly uncontaminated above $z = 2$. On the other hand, raising the magnitude threshold tends to reduce the relativistic corrections at all redshifts: we have checked that both evolution and magnification bias decreases in absolute values with increasing magnitude threshold, suggesting that future surveys with sensitivity to detect more fainter objects could also help with constructing tracer samples with reduced relativistic effects.

It is worth mentioning that for cosmological parameter inference from clustering measurements made on very large scales, the control of large-scale systematics should closely accompany the inclusion of relativistic corrections. For instance, the plane-parallel limit for power spectrum multipoles has been taken to simplify arguments in this work, but wide-angle effects due to variation of the line of sight have been shown to be critical on very large scales (Szalay et al. 1998; Szapudi 2004; Pápai & Szapudi 2008; Yoo & Seljak 2015). Therefore in a practical analysis, wide-angle corrections need to be included perturbatively (Castorina & White 2018; Beutler et al. 2019), or a spherical Fourier analysis could prove advantageous (Fisher et al. 1995; Heavens & Taylor 1995; Yoo & Desjacques 2013; Wang et al. 2020). Meanwhile, we have only considered quasars as a single tracer for detecting relativistic effects and the PNG signature in this work; to extract maximal information from future LSS probes, a multi-tracer approach can enhance the signal-to-noise ratio and thus prove more beneficial (McDonald & Seljak 2009; Seljak 2009).

6 CONCLUSION

Motivated by recent studies of relativistic effects in LSS observations and the prospect of constraining PNG through galaxy redshift surveys

to the level of precision competitive with CMB experiments in the near future, we have sought to quantify relativistic corrections to clustering statistics on very large scales, with quasars as a concrete example. These corrections do not only depend on the cosmological expansion history, but also on the redshift evolution of the underlying quasar number density and its sensitivity to the luminosity threshold, which are parametrized by evolution bias b_e and magnification bias s . To this end, we have refitted the eBOSS QSO luminosity function and derived measurements on both b_e and s , before propagating their constraints to relativistic corrections to the power spectrum multipoles. Our assessment of the impact of relativistic effects on the f_{NL} signature affirms the results of previous works mentioned in section 1, but this agreement is reached after a more realistic treatment for evolution and magnification bias contributions, in particular their uncertainties.

We have found that relativistic corrections can indeed be mistaken for f_{NL} -induced scale-dependent bias modifications, especially at low redshifts and in the power spectrum quadrupole. By using tracer samples at higher redshifts or with a fainter luminosity threshold, relativistic effects can be reduced to some extent. We have also found that, at least for the quasar population, the impact of evolution bias b_e and its uncertainties on clustering statistics is greater than that of magnification bias s . However, the latter also appears in lensing contributions to the observed galaxy over-density field, which we have neglected in this work and has been shown to be important for cosmological parameter inference (e.g. Lorenz et al. 2018; Jelic-Cizmek et al. 2020).

For future clustering measurements of the DESI quasar sample with apparent magnitude limit similar to the one considered in this work (DESI Collaboration, Aghamousa et al. 2016), relativistic corrections can be an order of magnitude larger than the modifications induced by $f_{\text{NL}} \approx 1$ on scales $k \sim 10^{-3} h^{-1} \text{Mpc}$ at lower redshifts

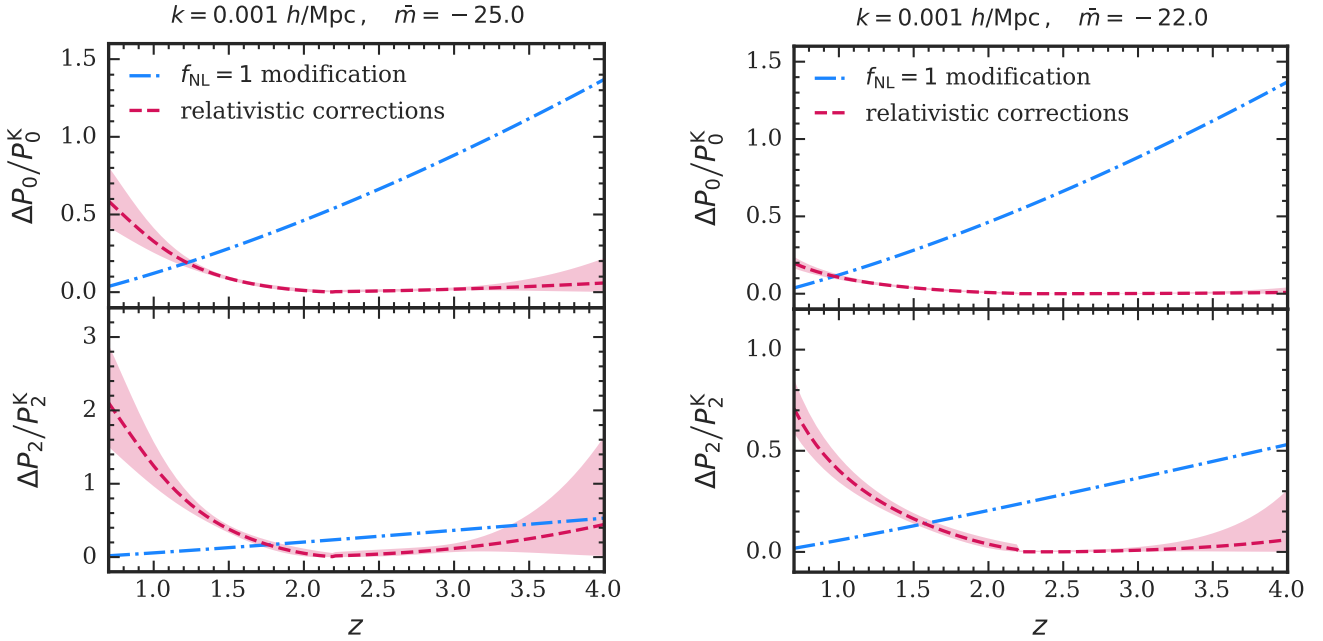


Figure 7. Scale-dependent modifications ΔP_ℓ to the quasar clustering power spectrum monopole and quadrupole as a fraction of the Kaiser RSD model P_ℓ^K at $k = 0.001 h^{-1} \text{Mpc}$ with absolute magnitude threshold $\bar{m} = -25$ (left column) and $\bar{m} = -22$ (right column). Relativistic corrections without local non-Gaussianity f_{NL} are shown by the dashed red lines with the shaded red regions showing the 95% credible interval derived from the best-fitting eBOSS QSO luminosity function in this work (see Table 1). Modifications due to $f_{\text{NL}} = 1$ (fiducial value) without relativistic corrections are shown by the dash-dotted blue lines.

$z \lesssim 1$; at higher redshifts $z \gtrsim 2.5$, relativistic corrections become significant again especially in the power spectrum quadrupole, where they can be up to 80% of the $f_{\text{NL}} \simeq 1$ modification at redshift $z \simeq 4$ for absolute magnitude threshold down to $\bar{m} = -25$. Therefore determining the tracer luminosity function and thus relativistic biases can be crucial to constraining local primordial non-Gaussianity, and we suggest that forward modelling of relativistic corrections should be fully included in such an analysis pipeline. For this purpose, we have made the code implemented in this work publicly available as a Python package, HORIZONGROUND⁸.

ACKNOWLEDGEMENTS

The authors would like to thank Obinna Umeh and Christophe Yèche for helpful discussions, and Nathalie Palanque-Delabrouille and Christophe Magneville for insights on the luminosity function fitting procedure. MSW would also like to thank Minas Karamanis for help with the MCMC sampling code ZEUS which is publicly available.

MSW is supported by the University of Portsmouth Student Bursary. FB is a Royal Society University Research Fellow. DB is supported by the UK STFC grant ST/S000550/1.

Numerical computations are performed on the Sciama High Performance Computing (HPC) cluster which is supported by the Institute of Cosmology and Gravitation (ICG), the South East Physics Network (SEPnet) and the University of Portsmouth. This work has made use of publicly available Python packages ASTROPY (Astropy Collaboration; Robitaille et al. 2013; Price-Whelan et al. 2018) and NBODYKIT (Hand et al. 2018).

⁸ github.com/MikeSWang/HorizonGround

REFERENCES

- Ade P. A. R. et al., 2016, *A&A*, 594, A13
Aghamousa A. et al., 2016, preprint (arXiv:1611.00036)
Akrami Y. et al., 2019, preprint (arXiv:1905.05697)
Alonso D., Bull P., Ferreira P. G., Maartens R., Santos M. G., 2015, *ApJ*, 814, 145
Alvarez M. et al., 2014, preprint (arXiv:1412.4671)
Amendola L. et al., 2018, *Living Rev. in Relativ.*, 21
Bertacca D., Maartens R., Raccanelli A., Clarkson C., 2012, *J. Cosmology Astropart. Phys.*, 2012, 025
Beutler F., Dio E. D., 2020, preprint (arXiv:2004.08014)
Beutler F., Castorina E., Zhang P., 2019, *J. Cosmology Astropart. Phys.*, 2019, 040
Bonvin C., Durrer R., 2011, *Phys. Rev. D*, 84, 063505
Bonvin C., Franco F. O., Fleury P., 2020, preprint (arXiv:2004.06457)
Boyle B. J., Shanks T., Croom S. M., Smith R. J., Miller L., Loaring N., Heymans C., 2000, *MNRAS*, 317, 1014
Bruni M., Crittenden R., Koyama K., Maartens R., Pitrou C., Wands D., 2012, *Phys. Rev. D*, 85, 041301
Camera S., Maartens R., Santos M. G., 2015, *MNRAS*, 451, L80
Castorina E., White M., 2018, *MNRAS*, 476, 4403
Castorina E. et al., 2019, *J. Cosmology Astropart. Phys.*, 2019, 010
Challinor A., Lewis A., 2011, *Phys. Rev. D*, 84, 043516
Conroy C., White M., 2012, *ApJ*, 762, 70
Croton D. J., 2009, *MNRAS*, 394, 1109
Dalal N., Doré O., Huterer D., Shirokov A., 2008, *Phys. Rev. D*, 77, 123514
Fisher K., Lahav O., Hoffman Y., Lynden-Bell D., Zaroubi S., 1995, *MNRAS*, 272, 885
Fonseca J., Camera S., Santos M. G., Maartens R., 2015, *ApJ*, 812, L22
Font-Ribera A., McDonald P., Mostek N., Reid B. A., Seo H.-J., Slosar A., 2014, *J. Cosmology Astropart. Phys.*, 2014, 023
Hand N., Feng Y., Beutler F., Li Y., Modi C., Seljak U., Slepian Z., 2018, *AJ*, 156, 160
Heavens A. F., Taylor A. N., 1995, *MNRAS*, 275, 483

- Jelic-Cizmek G., Lepori F., Bonvin C., Durrer R., 2020, preprint (arXiv:2004.12981)
- Jeong D., Schmidt F., Hirata C. M., 2012, *Phys. Rev. D*, 85, 023504
- Kaiser N., 1987, *MNRAS*, 227, 1
- Karamanis M., Beutler F., 2020, preprint (arXiv:2002.06212)
- Krolewski A. G., Eisenstein D. J., 2015, *ApJ*, 803, 4
- Laureijs R. et al., 2011, preprint (arXiv:1110.3193)
- Lorenz C. S., Alonso D., Ferreira P. G., 2018, *Phys. Rev. D*, 97, 023537
- Maldacena J., 2003, *J. High Energy Phys.*, 2003, 013
- Matarrese S., Verde L., 2008, *ApJ*, 677, L77
- McDonald P., Seljak U., 2009, *J. Cosmology Astropart. Phys.*, 2009, 007
- Mueller E.-M., Percival W. J., Ruggeri R., 2018, *MNRAS*, 485, 4160
- Palanque-Delabrouille N. et al., 2016, *A&A*, 587, A41
- Pápai P., Szapudi I., 2008, *MNRAS*, 389, 292
- Pozzetti L. et al., 2016, *A&A*, 590, A3
- Price-Whelan A. M. et al., 2018, *AJ*, 156, 123
- Raccanelli A., Montanari F., Bertacca D., Doré O., Durrer R., 2016, *J. Cosmology Astropart. Phys.*, 2016, 009
- Raccanelli A., Bertacca D., Jeong D., Neyrinck M. C., Szalay A. S., 2018, *Phys. Dark Univ.*, 19, 109
- Richards G. T. et al., 2006, *ApJ*, 131, 2766
- Robitaille T. P. et al., 2013, *A&A*, 558, A33
- Seljak U., 2009, *Phys. Rev. Lett.*, 102, 021302
- Shen Y., 2009, *ApJ*, 704, 89
- Shen Y. et al., 2013, *ApJ*, 778, 98
- Slosar A., Hirata C., Seljak U., Ho S., Padmanabhan N., 2008, *J. Cosmology Astropart. Phys.*, 2008, 031
- Szalay A. S., Matsubara T., Landy S. D., 1998, *ApJ*, 498, L1
- Szapudi I., 2004, *ApJ*, 614, 51
- Timlin J. D. et al., 2018, *ApJ*, 859, 20
- Wang M. S., Avila S., Bianchi D., Crittenden R., Percival W. J., 2020, in prep
- White M. et al., 2012, *MNRAS*, 424, 933
- Yoo J., Desjacques V., 2013, *Phys. Rev. D*, 88, 023502
- Yoo J., Seljak U., 2015, *MNRAS*, 447, 1789
- Yoo J., Fitzpatrick A. L., Zaldarriaga M., 2009, *Phys. Rev. D*, 80

This paper has been typeset from a \TeX/L\AA\TeX file prepared by the author.